3.1 Introduction

Environmental pollutant has become serious problem and organic substances such as synthetic dyes are the major source of contaminants causing threat to human health and ecological system. The requirement of specific technique for the detection of organic pollutant at low concentration is of utmost importance in order to protect public health [1]. One of the most versatile techniques that has the ability to identify molecules at deficient concentration levels is surface-enhanced Raman spectroscopy (SERS) [2–3]. Plasmonic nanomaterials (of noble metals) are used as adsorbates to amplify the Raman signals considerably to detect target molecules based on SERS. The well-known SERS methods of electromagnetic (EM) and chemical enhancement (CM) amplify the SERS signal of probe molecule acquired from the substrate. The enhanced-Raman signal using noble-metal nanostructures is vastly strong due to their size, strong SPR effect and morphology of substrate [3–4]. Recently, SERS has been demonstrated for the detection of organic pollutant using semiconducting materials instead of noble metals, especially after the report on TiO_2 [5] semiconducting nanoparticles with strong enhancement, more and more noble metal nanocomposite semiconductors are developed. Composites of noble and non-noble metals such as Ag/WO3 nanofiber (10^{-5} M, MB), ZnO/Ag and Ag/titania nanocomposites for the detection of RhB and 4-NP both at 10^{-4} M concentration level, and other semiconducting nanomaterials such as TiO2 nanocrystals, ZnO nanorod (10^{-3} M, MO), $MoO_3 \cdot xH_2O$ quantum dots (4×10^{-3} M hydrazine, 2.3×10^{-5} crystal violet) Ga-doped ZnO nanoparticles (10^{-3} M, MPy),

ZrO_2 nanoparticles, $K_2Ti_6O_{13}$ nanowires (10^{-3} M, 4-MBA) have been reported as active SERS substrate [6–13]. However, since the lack of reproducibility or stability in the SERS-active substrate has prevented the use of SERS as a common analytical tool, more and more researchers are increasingly interested in synthesizing innovative substrates to overcome these drawbacks. In this view, new material as bismuth NPs and bismuth thin film as SERS substrate have been performed to detect amino acids at concentration levels 5×10^{-3} M and rhodamine 6 G at 10^{-2} M respectively [14–15]. Towards this, bismuth based materials have been considered for potential SERS applications due to their chemical stability and fascinating optical properties as surface plasmon resonance tuned from UV− vis−NIR region [16]. Due to its great thermal stability, non-toxicity, and cost-effectiveness, bismuth oxybromide $Bi_{24}O_{31}Br_{10}$ has also received a lot of attention as a semiconducting photocatalyst for the degradation of organic contaminants [17].

In this work, a facile method for synthesis of $Bi_{24}O_{31}Br_{10}$ powders through chemical precipitation method is reported. Further, novel potential of $Bi_{24}O_{31}Br_{10}$ as an alternative SERS substrate for the detection of organic pollutants such as rhodamine B (RhB), 4-nitrophenol (4-NP) and methyl orange (MO) is also reported. Hitherto the detection of RhB, MO and 4-NP on bismuth-based substrate is not reported by others to the best of our knowledge. Overall, this bismuth based SERS substrate may be used as a complimentary substrate to the substrate as reported in chapter 2.

3.2 Experimental

3.2.1 Materials used

$Bi(NO_3)_3.5H_2O$, cetyltriethylammonium bromide (CTAB, SRL India). HNO_3, NaOH, rhodamine B, 4-nitrophenol, methyl orange, and ethanol were purchased from Merck, India. Without any prior treatment, all reagents were used as received. The solutions were made with double-distilled water.

3.2.2 Synthesis of Bismuth oxybromide ($Bi_{24}O_{31}Br_{10}$)

Bismuth oxybromide powders were synthesized through chemical precipitation method. In a typical procedure, 1.65 mmol of Bi $(NO_3)_3.5H_2O$ was dissolved in 16.70 mL of 1.6 M HNO_3, and 0.69 mmol of CTAB in 40 mL of aqueous 9.3 mmol NaOH were introduced as drops into the above acid solution with vigorous magnetic stirring at room temperature. The white precipitate was collected and washed with distilled water and ethanol three times, and dried in oven at 100 ºC for overnight. After that the dried sample was calcined at 500, 700 and 800 ºC for 2 h at the heating rate 15 ºC in a muffle furnace to obtain $Bi_{24}O_{31}Br_{10}$ powders based on previous study [17].

3.2.3 Characterization

SERS substrates were characterized via different techniques discussed in chapter 1.

3.2.4 SERS Measurement of substrate

Solutions of RhB in water (100 µM) and ethanol (100 µM to 20 µM), 4-NP and MO with a concentration of 1mM to 100 µM (in water) were used for the SERS detection. Raman spectra were collected from 100 µl of analyte solution deposited on the surface of the bismuth oxybromide NPs taken on a glass slide and dried in air before the measurement. SERS spectra of RhB and 4-NP were recorded with integration time of 5s. The SERS signals of 10^{-4} M of MO on surface were collected under the exposure time of 20s. Raman and SERS activity measurement of substrate was conducted under a laser power of 100 mW with excitation wavelength was 785 nm (Research India) and more technical details are given in chapter 1, section 1.6.6.

3.3 Results and Discussion

3.3.1 XRD-pattern

The crystal structure and formation of synthesized $Bi_{24}O_{31}Br_{10}$ powders calcined at 500, 700 and 800 ºC were confirmed by X-ray diffraction measurement as illustrated in **Figure 3.1**. The XRD patterns of the sample exhibited the characteristic peaks (in degree) at 10.6, 21.3, 24.1, 29.0, 29.8, 31.1, 31.8, 37.0, 39.8, 43.2, 45.4, 48.8, 50.6, 53.1, 54.6, 55.8, 57.0, 66.5 of monoclinic structure corresponding to reflection planes $(102), (20\bar{4}), (11\bar{1}), (30\bar{4}), (213), (11\bar{1}0), (117), (10\bar{1}2), (40\bar{6}), (1114), (0113), (12\bar{4}), (419), (320), (324), (12\bar{1}0), (011), (2214)$, respective, in good agreement with JCPDS card no. 75–0888. XRD analysis reveals the monoclinic and

crystalline nature of the synthesized $Bi_{24}O_{31}Br_{10}$. **Figure 3.1** demonstrates that the intensity of XRD peaks increases with increase in annealing temperature at 500, 700 and 800 ºC, which indicate the phase stability of $Bi_{24}O_{31}Br_{10}$ samples.

The crystalline size of particles was calculated using the Debye–Scherrer formula [18] using equation 1.20. The average crystalline size of $Bi_{24}O_{31}Br_{10}$ powders at different temperature 500, 700 and 800 ºC are 19.64, 24.83 and 30.69 nm, respectively.

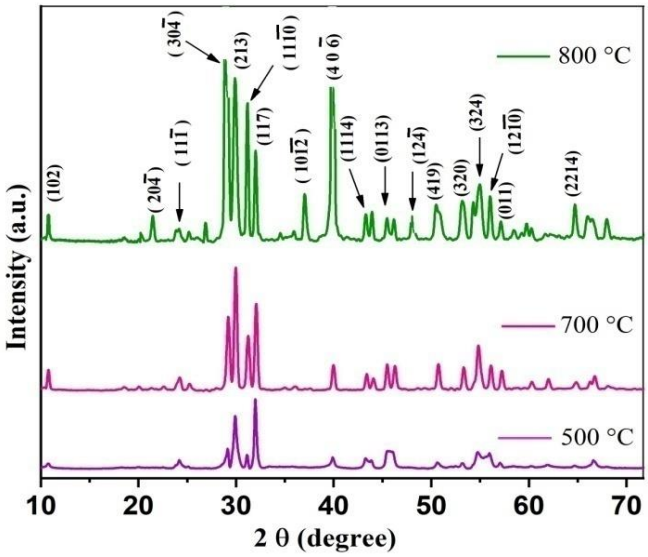

Figure 3.1 *XRD pattern of $Bi_{24}O_{31}Br_{10}$ calcined at 500, 700 and 800 ºC.*

3.3.2 SEM analysis

The morphology of the synthesized samples was studied by scanning electron microscope (SEM) at different magnification as display in **Figure 3.2**. **Figure 3.2 (a)** illustrates the SEM image of the prepared sample $Bi_{24}O_{31}Br_{10}$ calcined at 500 ºC, wheremost of the particles have rod like structure with average length of 10.9 μm. When the annealing temperature was increased to 700 and 800 ºC

agglomeration was observed. As shown in **Figure 3.2(b)**, it was observed that (sample at 700 ºC) particles have rod as well as plate-like structure with the average length of 6.4 and 3.5 μm, respectively. **Figure 3.2(c)** shows agglomerated rod like structure of $Bi_{24}O_{31}Br_{10}$ calcined at 800 ºC with average length of 12.8 μm. It is obvious as the calcinations temperature increases morphologies developed from rod-like to agglomerated rod like shape.

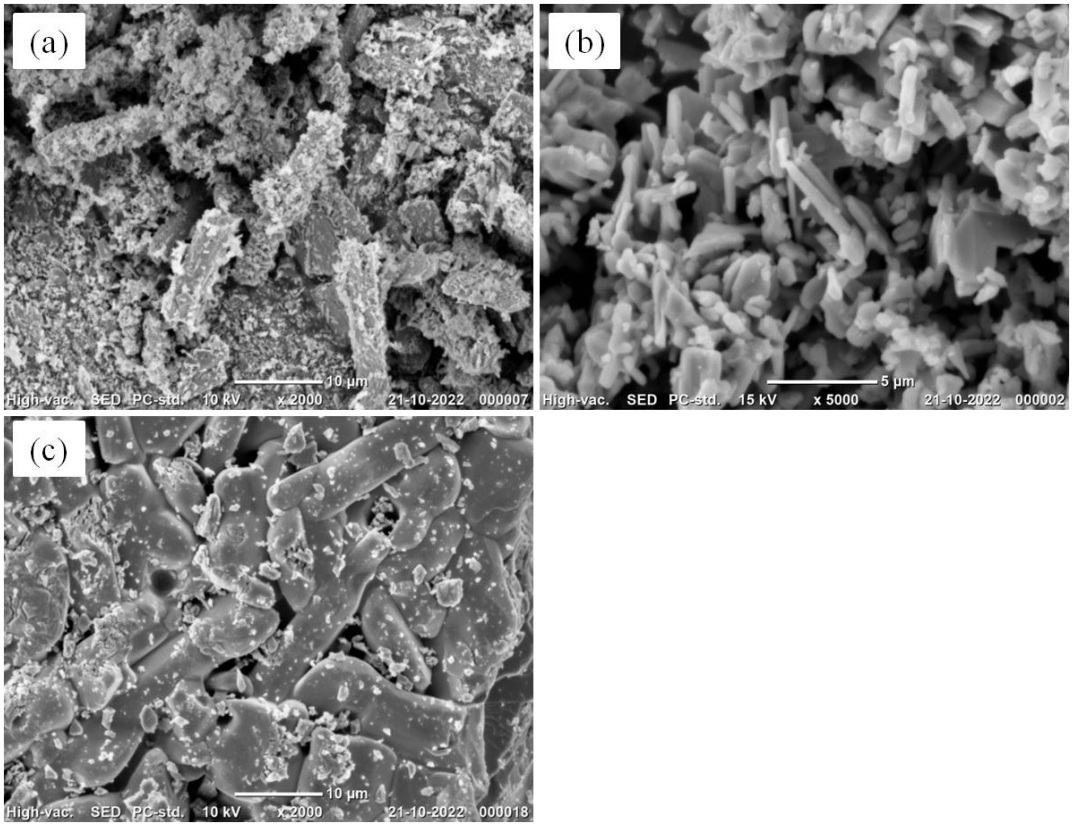

Figure 3.2 *SEM image of $Bi_{24}O_{31}Br_{10}$ powders calcined at different temperature (a) 500 ºC (b) 700 ºC and (c) 800 ºC.*

3.3.3 XPS analysis

XPS analysis was carried out to understand the elemental composition and chemical states of the synthesized $Bi_{24}O_{31}Br_{10}$ powders as depicted in **Figure 3.3**. **Figure 3.3 (a)** shows the survey scan spectrum which confirmed the presence of bismuth, oxygen, bromine elements in the synthesized sample. The appearance of C1s at 284.9 eV can be attributed to adventitious carbon species from XPS measurement [19].

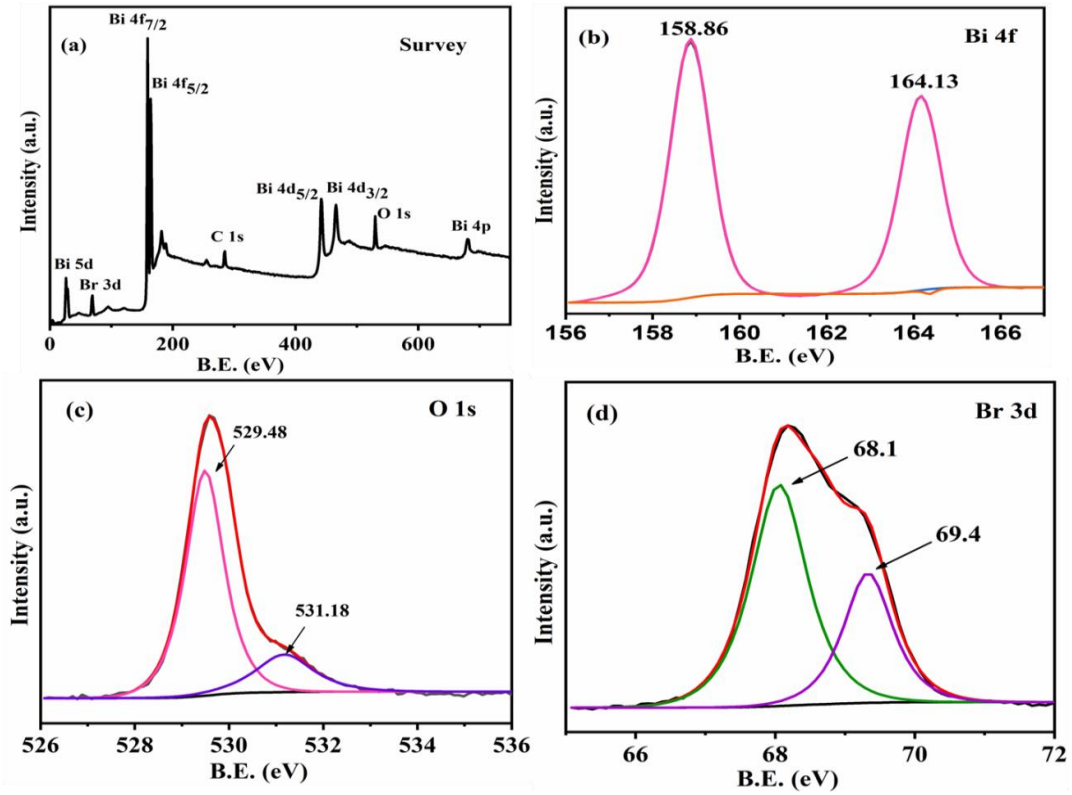

Figure 3.3 *XPS spectra for $Bi_{24}O_{31}Br_{10}$ at 500 ºC (a) XPS survey spectra (b) Bi 4f (c) O 1s (d) Br 3d.*

The peaks as shown in **Figure 3.3 (b)** represents the Bi 4f spectrum where the peaks of Bi $4f_{7/2}$ and Bi $4f_{5/2}$ are located at 158.86 and 164.13 eV, respectively, indicate that

Bi ion exists as Bi^{3+} in the prepared sample [20]. The XPS spectra of O1s with the peak at binding energy of 529.6 eV, attributed to bismuth oxygen bond and the peak at 531.18 eV corresponds to adsorbed H_2O on surface as shown in **Figure 3.3 (c)** [20, 22]. In the Br 3d spectrum (**Figure 3.3 (d)**), the binding energy peaks at 68.1 and 69.4 eV are ascribed to Br $3d_{3/2}$ and Br $3d_{5/2}$ of Br, respectively in $Bi_{24}O_{31}Br_{10}$ [20, 23].

Further, XPS analysis confirmed the formation of $Bi_{24}O_{31}Br_{10}$ powders. It is gleaned from literature that oxygen rich bismuth oxybromide ($Bi_{24}O_{31}Br_{10}$) is thermally more stable compared to BiOBr and has higher optical activity [17]. It is also gathered from literature that the combination of Au with bismuth oxyiodide has higher SERS activity as compared to BiOI and the Au coated BiOI has been used as substrate to investigate SERS activity where concentration levels as low as 5 μM of R6G analyte on Au−BiOI substrate was achieved [23]. Based on these reports, it is deduced that $Bi_{24}O_{31}Br_{10}$ may provide an enhanced SERS performance.

3.3.4 Vibrational Raman spectra

Raman spectroscopy has been used frequently to examine bismuth oxybromide samples in order to get the distinctive peaks in the region of 100-400 cm^{-1} [24]. Authors have, nevertheless, noted in the literature that bismuth oxybromide has vibrational Raman modes that are close to 500 cm^{-1} [25]. However, the Raman mode of the $Bi_{24}O_{31}Br_{10}$ sample's distinctive mode of vibration above 400 cm^{-1} is not well understood. Here, Raman spectra of the as-synthesized $Bi_{24}O_{31}Br_{10}$

powders were calcined at various temperatures was observed in the 400-1200 cm^{-1} region as depicted in **Figure 3.4 (a)**. The peaks at 453, 511 and 594 cm^{-1} may be ascribed to stretching modes of Bi-O in $Bi_{24}O_{31}Br_{10}$ which are its characteristic modes of vibrations [25].

In accordance with Gaussian fitted Raman spectrum of $Bi_{24}O_{31}Br_{10}$ (**Figure 3.4 (b-d)**), it was observed that at 500 ºC the intensity ratio of the peaks I_{453}/I_{511} and I_{594}/I_{511} are 0.75 and 0.25, at 700 ºC are 1 and 0.85 respectively, whereas at 800 ºC the intensity ratio of the modes I_{453}/I_{511} and I_{594}/I_{511} are 1 and 1.05 respectively. Further, we observed the variation in full width at half maxima (FWHM) with respect to most intense peak in the Raman spectrum. It was found that $FWHM_{500}$> $FWHM_{700}$> $FWHM_{800}$ corresponding to the calcinations at 500, 700, 800 ºC for $Bi_{24}O_{31}Br_{10}$ powders. It is therefore inferred that with the increase in temperature the ratio of Raman intensity increases and no significant shift in peaks were observed, which demonstrate the thermal stability and stable phase of the sample which is in accordance with the previously reported study [17].

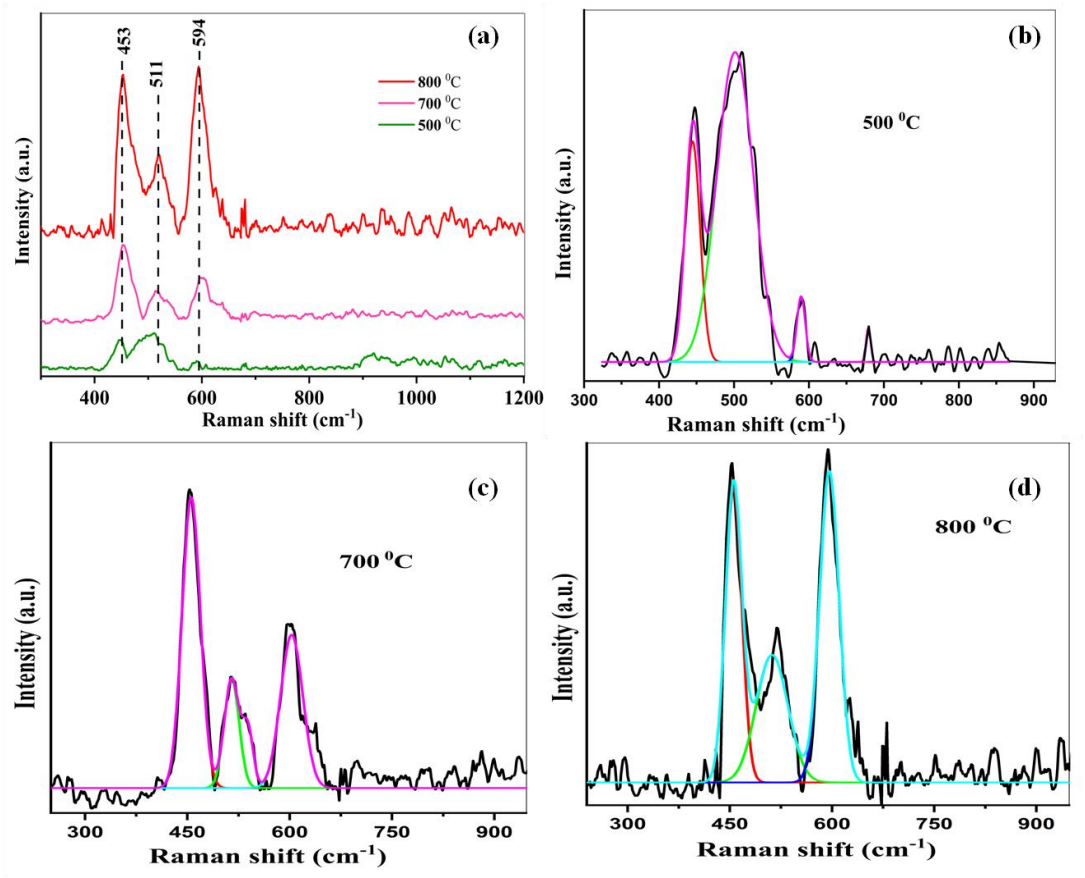

Figure 3.4 *(a) Raman spectra of* $Bi_{24}O_{31}Br_{10}$ *powders after annealing at different temperature and Gaussian fitted Raman spectra at (b) 500, (c) 700 and (d)800°C.*

3.3.5 SERS measurement of $Bi_{24}O_{31}Br_{10}$

To perform the SERS activity of $Bi_{24}O_{31}Br_{10}$ substrate calcined at different temperature at 500, 700, and 800 ºC standard probe molecule RhB was selected. Further provide an evidence of its SERS activity another analytes 4-NP and MO was also utilized, and explored by the comparison of the measured SERS spectrum with respect to their aqueous and solid normal Raman spectrum. The observed Raman peaks for the probe molecules with their tentative assignment illustrated in **Table**

3.1.

As shown in **Figure 3.5 (a)**, Raman spectrum of RhB in solid state was recorded to match their respective position of the peaks in the SERS spectra and their assignments are listed in **Table 3.1**. The SERS spectra of ethanolic RhB at concentration level 500 µM on $Bi_{24}O_{31}Br_{10}$ substrate calcined at different temperatures are shown in **Figure 3.5 (c)**.

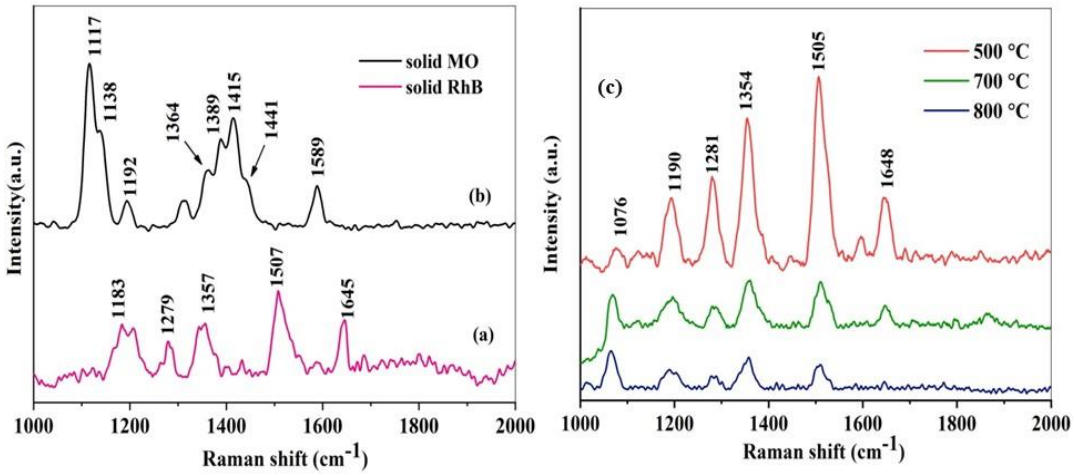

Figure 3.5 *Raman spectra of (a) solid RhB, and (b) solid MO, and (c) SERS spectra of ethanolic RhB (500 µM) on* $Bi_{24}O_{31}Br_{10}$ *substrate at different temperature.*

In the SERS spectrum, the significant enhancement in Raman signal of RhB was observed on substrate calcined at 500 ºC, but $Bi_{24}O_{31}Br_{10}$ substrates continuing the calcinations at 700, 800 ºC showed appreciable decline in SERS response of RhB. Therefore, $Bi_{24}O_{31}Br_{10}$ powder calcined at 500 ºC used as SERS substrate for further study.

Figure 3.6 (a-b) shows SERS spectrum of RhB on $Bi_{24}O_{31}Br_{10}$ substrate (at

500 ºC) in different solvent such as water and ethanol solution with the characteristic vibrational modes observed at 1076, 1190, 1281, 1354, 1505, 1525, 1648 cm^{-1}. RhB detection by SERS can be significantly impacted by the solvent and surface morphology of substrate [26]. When the SERS spectra of 100 μM RhB in both solutions was recorded, it was found that the RhB solution in ethanol on the $Bi_{24}O_{31}Br_{10}$ substrate has significantly greater enhancement ability than the aqueous RhB on the $Bi_{24}O_{31}Br_{10}$ substrate. The most intense peaks on substrate were observed at 1190 cm^{-1} (C-C vibrational mode), 1281 cm^{-1} (C-H bending), 1354, 1505 cm^{-1} (C-C bending) [27]. All the observed SERS peaks are in accordance with the characteristic peaks of RhB reported in the literature and the peak at 1076 cm^{-1} got significant enhancement in SERS spectra due to the interaction of probe with SERS substrate.

The amplified SERS signals reveal that ethanolic RhB has a strong adsorption affinity on substrate even at the low concentration. The SERS potential for $Bi_{24}O_{31}Br_{10}$ powders was performed with a lower detection limit of 20 μM of RhB in ethanol (**Figure 3.6 (b)**) compared to 100 μM for aqueous solution of RhB (**Figure 3.6 (a)**). This indicates that the SERS results may be tuned by the solvent.

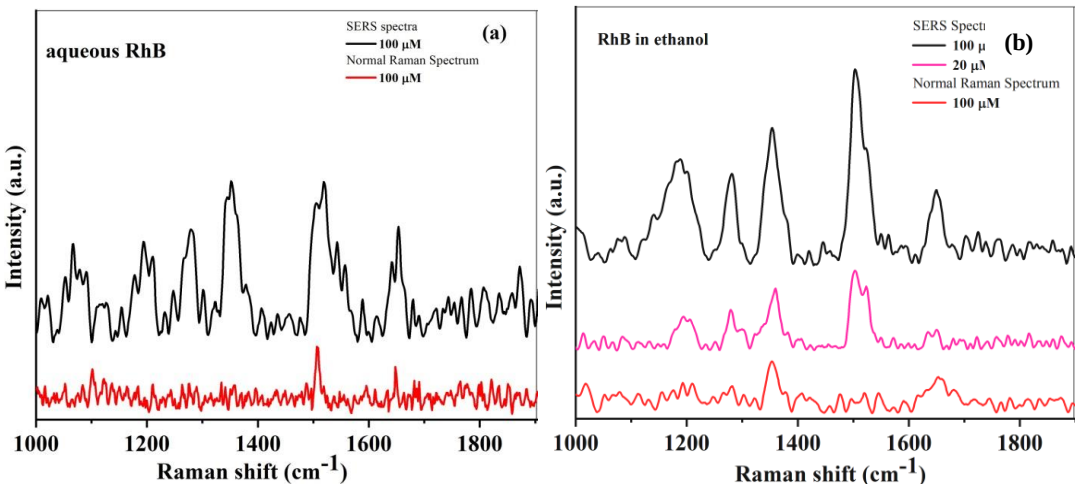

Figure 3.6 *SERS spectra of RhB solution (a) aqueous (b) ethanol on* $Bi_{24}O_{31}Br_{10}$ *substrate.*

Figure 3.7 (a) shows the Raman peaks were observed at 863, 1105, 1163, 1212, 1276, 1322, 1513, 1586 cm^{-1} for 4-nitrophenol (4-NP) molecule and the detailed assignment of vibrational peaks of 4-NP are shown in **Table 3.1**. The characteristic peaks of 4-NP were clearly observed from SERS spectra (**Figure 3.7 (b)**) over the $Bi_{24}O_{31}Br_{10}$ substrate. After exposure to a 785 nm laser excitation source, intensities of all Raman peaks rapidly increased. The most intense peak appeared at 1327 cm^{-1} is ascribed to the NO_2 symmetric stretching mode. Other sharp peaks at 1105 $cm^{-1}$and blue shift at 1282 cm^{-1} was observed corresponding to C-H in plane bend due to the adsorption of probe on substrate. The highlighted peaks in the SERS spectrum have less intensity, where the peaks at 1209 and1157 cm^{-1} exhibits red shift compared to Raman spectrum of solid 4-NP, can be attributed to O-C stretch and C-H in plane bend, which is in agreement with the reported value in literature[7]. Hence, the quantitative determination of organic pollutant is expected to be a

promising potential for the development of enhanced performance of bismuth-based SERS substrate.

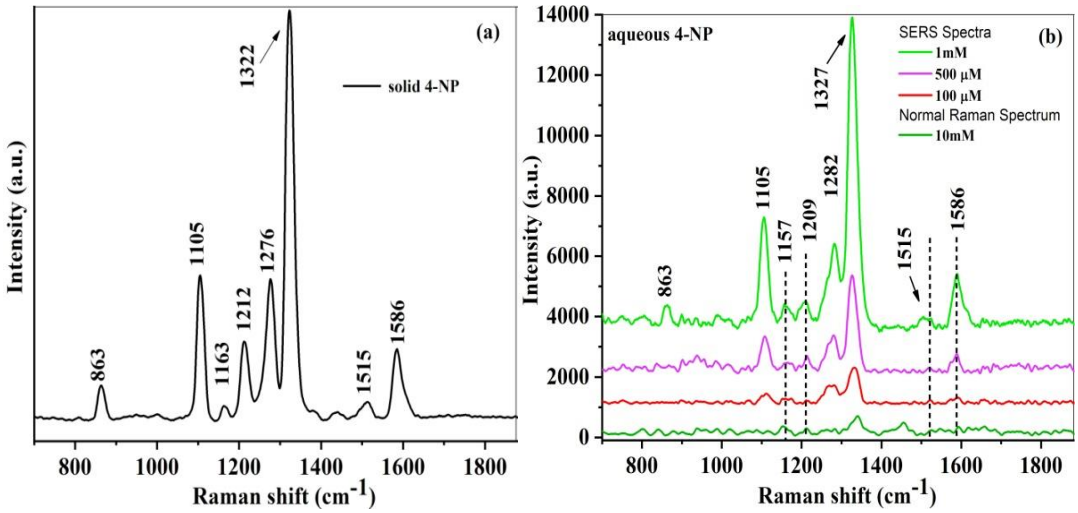

Figure 3.7 *(a) Raman spectra of solid and 10 mM aqueous 4-nitrophenol (4-NP) (b) SERS spectra of 4-nitrophenol on* $Bi_{24}O_{31}Br_{10}$ *substrate.*

Further, MO was analyzed on bismuth oxybromide substrate quantitatively. Raman spectrum of MO in solid state is shown in **Figure 3.5 (b)** and the normal Raman spectra of 1mM aqueous MO displayed in **Figure 3.8**. The SERS activity of MO from 1mM to 100 μM over $Bi_{24}O_{31}Br_{10}$ powders substrate is shown in **Figure 3.8**, where strong bands at 1117, 1140, 1192, 1366, 1392, 1419, 1447 and 1592 cm^{-1}can be clearly observed and these are in good agreement with the characteristic Raman peaks of MO reported in the literature [28–29]. The detection limit of MO was determined to be 10^{-4} M. As a result, it is evident that $Bi_{24}O_{31}Br_{10}$ can serve as a substrate for high-activity SERS.

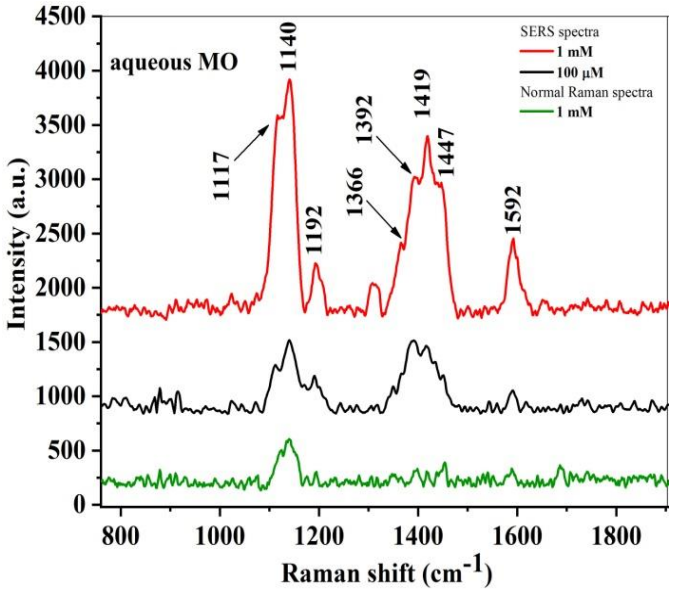

Figure 3.8 *Normal Raman spectra of 1mM aqueous MO and SERS spectra of MO (1mM, 100 μM) on* $Bi_{24}O_{31}Br_{10}$ *substrate.*

Nevertheless, semiconducting SERS materials including metal oxides, and a variety of doped or nanocomposite semiconductor-based SERS substrates, such as Ag/WO3, ZnO/Ag, Ag/titania, Ga-doped ZnO, were prepared, and examined for their SERS ability, with the detection limit in the range of 10^{-3} to 10^{-5} M [10–14]. Similar to these metal oxides, bismuth oxybromide powders are also one of the most promising substrates to be used in SERS application because they exhibit excellent SERS activity, stability, and have a lower detection limit than the metal substrates for the detection of organic pollutants that have been previously reported [23].

In order to verify the stability of the prepared substrate, RhB ethanolic solution with 10^{-4} M concentration was used as a probe molecule and SERS spectra was collected from twelve randomly selected positions on $Bi_{24}O_{31}Br_{10}$ substrate under the same experimental condition. As shown in **Figure 3.9 (a)** there is almost

similar SERS spectra with relative standard deviation (RSD) (shown alongside) in acceptable range. The relative standard deviation (RSD) of SERS peak around 1505 cm^{-1} was performed to estimate the reproducibility of SERS signal, and the RSD was calculated to be 9.40% as shown in **Figure 3.9 (b)**. These results demonstrate that bismuth oxybromide powder has excellent stability at different positions, and can be used as an excellent SERS substrate.

Moreover, $Bi_{24}O_{31}Br_{10}$ powders were used to demonstrate multi-molecule detection ability, and the probe molecules were 10^{-4} M of RhB in ethanol, 10^{-3} M of methyl orange (MO), and 10^{-3} M of 4-NP. From **Figure 3.9 (c)**, it can be observed that the characteristic peaks of probe molecules RhB at 1281, 1505, 1648 cm^{-1}, MO at 1117, 1419, 1592 cm^{-1}, and 4-NP at 1322, 1586 cm^{-1} can be well distinguished in the SERS spectra of mixed solution, indicating that the bismuth oxybromide substrate is also good for multi-molecular detection.

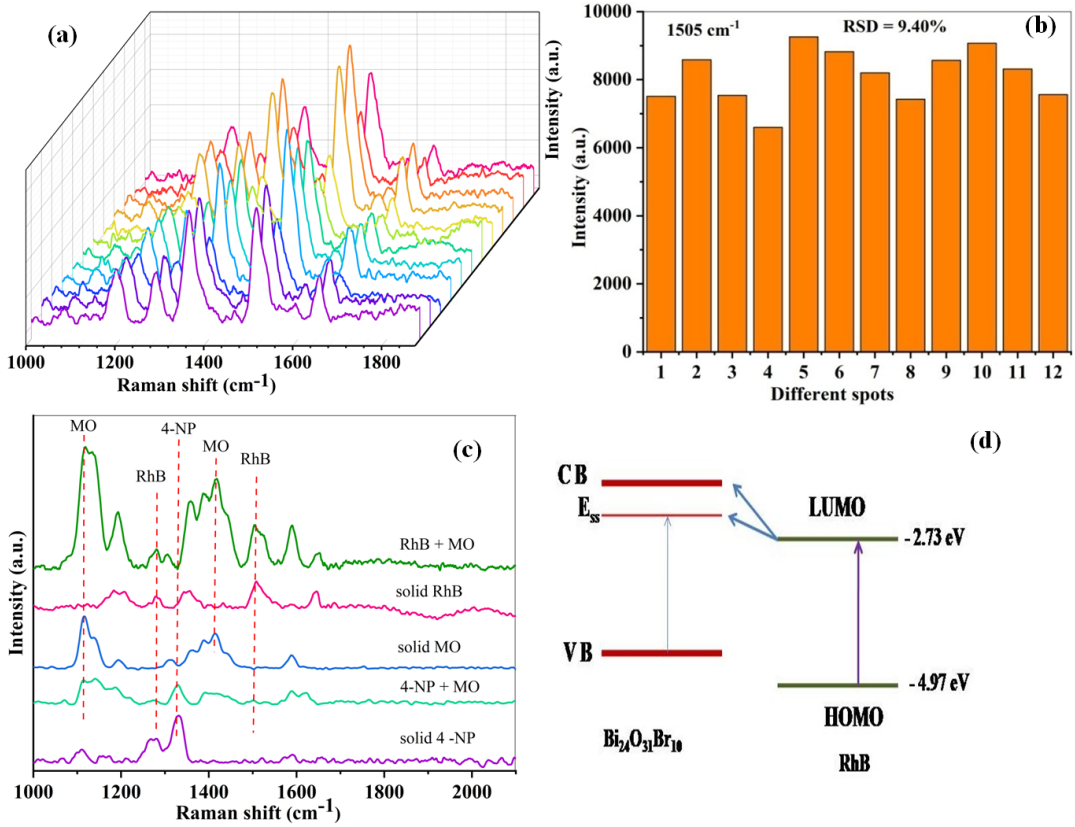

Figure 3.9 *(a) SERS spectra of 10^{-4} M RhB from 12 randomly selected positions (b) Relative standard deviation (RSD) at 1505 cm^{-1} (c) multi-molecule detection on $Bi_{24}O_{31}Br_{10}$ substrate (d) Charge transfer process in bismuth oxybromide system.*

Enhancement Factor

The enhancement factor was estimated utilizing RhB, 4-NP, and MO as probe molecules to demonstrate the effectiveness of $Bi_{24}O_{31}Br_{10}$ SERS substrate. The expressionin equation was used to determine the enhancement factor for SERS measurements [30]. The SERS enhancement factors (EF) for considered molecule over $Bi_{24}O_{31}Br_{10}$ powders acquired by measuring relative Raman intensities were 7.8×10^4 for RhB, 5.7×10^3 for 4-NP, and 3.8×10^3 for MO corresponding to

most prominent peaks 1505, 1327, and 1140 cm^{-1} respectively.

In addition, RhB was selected as a probe molecule on this substrate to understand the SERS mechanism. As mentioned earlier in chapter 1, there are two mechanisms to interpret the Raman enhancement i.e., electromagnetic (EM), and chemical (CM) enhancement mechanism [3]. EM is due to the electric field caused by surface plasmon resonance of nanomaterials by incident radiation. The enhancement factor for EM can contribute above 10^4, and reach to more than 10^{10}. Like noble metals, some semiconductors also show plasmon resonance in infrared region [31]. In the case of bismuth oxybromide semiconductor there is a possibility of EM enhancement at 785 nm incident laser. However previous studies demonstrate that chemical enhancement is predominant for enhancement in bismuth based materials [14].

Chemical enhancement is associated with chemisorption, and photo-induced charge transfer, which contributed to the increases the Raman scattering cross section when more charge separation occurs inside the molecules, and thereby increasing the polarizability of molecules. The schematic diagram in **Figure 3.9 (d)** shows the photo-induced charge transfer mechanism for the CM enhancement. In this system charge transfer (CT) process occurs between bismuth oxybromide, and adsorbed RhB molecules. The highest occupied molecular orbit (HOMO), and the lowest unoccupied molecular orbit (LUMO) level of RhB molecule are -4.97, and -2.73 eV, respectively and the energy gap is 2.24 eV [32] as shown in Figure 3.9 (d). The band gap of $Bi_{24}O_{31}Br_{10}$ between valence band (VB), and conduction

band (CB) is 2.77 eV [17], which is higher than the incident light 785 nm (1.58 eV), and thus, the probability of electron transition from VB to CB is less. When laser light incident on RhB molecule adsorbed on $Bi_{24}O_{31}Br_{10}$, the RhB molecule exhibits charge transfer process. Electrons from the HOMO of the adsorbed RhB molecule are excited to the LUMO, and electrons excited from LUMO to surface state energy levels (E_{ss}), and then photo-induced electrons transfer into $Bi_{24}O_{31}Br_{10}$ CB plausibly occurs. Apart from this, solvent (ethanolic RhB) has significant role in SERS enhancement mechanism through chemical enhancement, where solvent (ethanol) induces the charge separation between the adsorbed molecule, and substrate that promotes the non-resonance enhancement between them in charge transfer process by incident laser light [32].

3.4 Conclusion

The chemical precipitation procedure was successfully used to synthesize $Bi_{24}O_{31}Br_{10}$ powders. Raman spectrum for as-prepared samples was obtained to be single phase from low to higher temperature. The observed results demonstrate that $Bi_{24}O_{31}Br_{10}$ powders showed higher SERS activity when calcined at 500 ºC. The SERS activity of $Bi_{24}O_{31}Br_{10}$ substrate was proven by the adsorption of organic dyes RhB, 4-NP, and MO on it. The detection limit as low as 20 μM for RhB, 100 μM for 4-NP, and MO were obtained. The SERS detection of various dyes demonstrates the efficient SERS activity of substrate that can take the place of conventional SERS substrate. This research opens up the possibility of investigating the creation of SERS substrates based on materials containing bismuth.

Table 3.1 Tentative assignment for considered Raman modes of analytes RhB, 4-NP, MO (ν = stretching, as = anti-symmetric, δ = bending, ip = in plane, ph = phenyl)

Analyte	**Raman shift (cm^{-1})**	**Assignment**
RhB	1076 1190 1281 1354, 1505 1525 1648	ν(C−H) C−C bridge band stretching and aromatic δ(C−H) aromatic δ(C−C) ν(C−H) aromatic ν(C−H) Ref [27]
4-NP	863 1105/1163/1276 1212 1322 1513 1586	$\delta(NO_2)$ δip (C-H) ν (O-C) ν_{as}(NO2) ν_{as} (NO_2) Ring stretch Ref [7]
MO	1117/1192 1138 1364 1389/1415 1441/1589	*ν* (Ph–N) *δ* (C–H) *ν* (C–C) *ν*(Ph–N) *ν* (N=N) *ν* (C–C) Ref [29-30]

References:

[1] V. S. Tran *et al.*, "Typical low cost biosorbents for adsorptive removal of specific organic pollutants from water," *Bioresour. Technol.*, vol. 182, pp. 353–363, 2015, doi: 10.1016/j.biortech.2015.02.003.

[2] R. A. Alvarez-Puebla and L. M. Liz-Marzán, "Traps and cages for universal SERS detection," *Chem. Soc. Rev.*, vol. 41, no. 1, pp. 43–51, 2012, doi: 10.1039/C1CS15155J.

[3] P. J. Arathi, S. Bhaskar, G. Rajendra Kumar Reddy, P. Suresh Kumar, and V. Ramanathan, "The photocatalytic role of electrodeposited copper on pencil graphite," *Phys. Chem. Chem. Phys.*, vol. 20, no. 5, pp. 3430–3432, 2018, doi: 10.1039/c7cp08383a.

[4] J. Kneipp, H. Kneipp, and K. Kneipp, "SERS—a single-molecule and nanoscale tool for bioanalytics," *Chem. Soc. Rev.*, vol. 37, no. 5, pp. 1052–1060, 2008, doi: 10.1039/B708459P.

[5] A. Musumeci *et al.*, "SERS of semiconducting nanoparticles (TiO2 hybrid composites)," *J. Am. Chem. Soc.*, vol. 131, no. 17, pp. 6040–6041, 2009.

[6] C. H. Sun, M. L. Wang, Q. Feng, W. Liu, and C. X. Xu, "Surface-enhanced Raman scattering (SERS) study on Rhodamine B adsorbed on different substrates," *Russ. J. Phys. Chem. A*, vol. 89, no. 2, pp. 291–296, 2015, doi: 10.1134/S0036024415020338.

[7] M. Muniz-Miranda, "SERS monitoring of the catalytic reduction of 4-nitrophenol on Ag-doped titania nanoparticles," *Appl. Catal. B Environ.*, vol. 146, pp. 147–150, 2014, doi: 10.1016/j.apcatb.2013.03.008.

[8] L. Liu, F. Pan, C. Liu, L. Huang, W. Li, and X. Lu, "TiO2 Nanofoam–Nanotube Array for Surface-Enhanced Raman Scattering," *ACS Appl. Nano Mater.*, vol. 1, no. 12, pp. 6563–6566, Dec. 2018, doi: 10.1021/acsanm.8b01566.

[9] S. Lee, J.-W. Peng, and C.-S. Liu, "Photoluminescence and SERS investigation of plasma treated ZnO nanorods," *Appl. Surf. Sci.*, vol. 285, no. PARTB, pp. 748–754, 2013, doi: 10.1016/j.apsusc.2013.08.120.

[10] Y. Wang *et al.*, "Surface Plasmon Resonance from Gallium-Doped Zinc Oxide Nanoparticles and Their Electromagnetic Enhancement Contribution to Surface-Enhanced Raman Scattering," *ACS Appl. Mater. Interfaces*, vol. 13, no. 29, pp. 35038–35045, Jul. 2021, doi: 10.1021/acsami.1c05804.

[11] G. Song *et al.*, "Quantum Effects Enter Semiconductor-Based SERS: Multiresonant MoO3·xH2O Quantum Dots Enabling Direct, Sensitive SERS Detection of Small Inorganic Molecules," *Anal. Chem.*, vol. 94, no. 12, pp. 5048–5054, Mar. 2022, doi: 10.1021/acs.analchem.1c05142.

[12] P. Ji *et al.*, "Improved Surface-Enhanced Raman Scattering Properties of ZrO2 Nanoparticles by Zn Doping," *Nanomaterials*, vol. 9, no. 7. 2019. doi: 10.3390/nano9070983.

[13] L. Chen *et al.*, "High-efficiency charge transfer on SERS-active semiconducting K2Ti6O13 nanowires enables direct transition of photoinduced electrons to protein redox centers," *Biosens. Bioelectron.*, vol. 191, 2021, doi: 10.1016/j.bios.2021.113452.

[14] A. G. Bezerra, P. Cavassin, T. N. Machado, T. D. Woiski, R. Caetano, and W. H. Schreiner, "Surface-enhanced Raman scattering using bismuth nanoparticles: a study with amino acids," *J. Nanoparticle Res.*, vol. 19, no. 11, 2017, doi: 10.1007/s11051-017-4057-6.

[15] *R.M. Philip, D.B. Mohan Mater. Today. Proc., 46 (2021), pp. 2945-2949.*

[16] Z. Wang, C. Jiang, R. Huang, H. Peng, and X. Tang, "Investigation of Optical and Photocatalytic Properties of Bismuth Nanospheres Prepared by a Facile Thermolysis Method," *J. Phys. Chem. C*, vol. 118, no. 2, pp. 1155–1160, Jan. 2014, doi: 10.1021/jp4065505.

[17] J. Shang *et al.*, "Bismuth Oxybromide with Reasonable Photocatalytic Reduction Activity under Visible Light," *ACS Catal.*, vol. 4, no. 3, pp. 954–961, Mar. 2014, doi: 10.1021/cs401025u.

[18] B. D. Cullity, *Elements of X-ray Diffraction*. Addison-Wesley Publishing, 1956.

[19] J. Song, L. Zhang, J. Yang, X.-H. Huang, and J.-S. Hu, "Hierarchical porous Bi24O31Br10microarchitectures assembled by ultrathin nanosheets with strong

adsorption and excellent photocatalytic performances," *Mater. Des.*, vol. 123, pp. 128–136, 2017, doi: 10.1016/j.matdes.2017.03.046.

[20] Y. Guo, Y. Zhang, N. Tian, and H. Huang, "Homogeneous {001}-BiOBr/Bi Heterojunctions: Facile Controllable Synthesis and Morphology-Dependent Photocatalytic Activity," *ACS Sustain. Chem. Eng.*, vol. 4, no. 7, pp. 4003–4012, Jul. 2016, doi: 10.1021/acssuschemeng.6b00884.

[21] B. Xiao, W. Zhao, Y. Xiang, X. Wu, and G. Zhang, "Vis-NIR responsive Bi24O31Br10 and corresponding composite with up-conversion phosphor towards efficient photocatalytic oxidation," *Appl. Surf. Sci.*, vol. 489, pp. 210–219, 2019, doi: 10.1016/j.apsusc.2019.05.355.

[22] C.-Y. Wang, X. Zhang, H.-B. Qiu, G.-X. Huang, and H.-Q. Yu, "Bi24O31Br10 nanosheets with controllable thickness for visible–light–driven catalytic degradation of tetracycline hydrochloride," *Appl. Catal. B Environ.*, vol. 205, pp. 615–623, 2017, doi: 10.1016/j.apcatb.2017.01.015.

[23] M. D. Prasad, M. G. Krishna, and S. K. Batabyal, "Facet-Engineered Surfaces of Two-Dimensional Layered BiOI and Au–BiOI Substrates for Tuning the Surface-Enhanced Raman Scattering and Visible Light Photodetector Response," *ACS Appl. Nano Mater.*, vol. 2, no. 6, pp. 3906–3915, Jun. 2019, doi: 10.1021/acsanm.9b00771.

[24] D. Wu *et al.*, "Boron doped BiOBr nanosheets with enhanced photocatalytic inactivation of Escherichia coli," *Appl. Catal. B Environ.*, vol. 192, pp. 35–45, 2016, doi: 10.1016/j.apcatb.2016.03.046.

[25] R. Li *et al.*, "In situ reorganization of Bi3O4Br nanosheet on the Bi24O31Br10 ribbon structure for superior visible-light photocatalytic capability," *Sep. Purif. Technol.*, vol. 247, 2020, doi: 10.1016/j.seppur.2020.117007.

[26] X. Zu *et al.*, "Surface-enhanced Raman scattering effect of ordered gold nanoparticle array for rhodamine B with different morphologies," *Chinese J. Polym. Sci.*, vol. 33, no. 10, pp. 1470–1476, 2015, doi: 10.1007/s10118-015-1690-3.

[27] J. Zhang, X. Li, X. Sun, and Y. Li, "Surface Enhanced Raman Scattering Effects

of Silver Colloids with Different Shapes," *J. Phys. Chem. B*, vol. 109, no. 25, pp. 12544–12548, Jun. 2005, doi: 10.1021/jp050471d.

[28] M. Z. Si, Y. P. Kang, and Z. G. Zhang, "Surface-enhanced Raman scattering (SERS) spectra of Methyl Orange in Ag colloids prepared by electrolysis method," *Appl. Surf. Sci.*, vol. 255, no. 11, pp. 6007–6010, 2009, doi: 10.1016/j.apsusc.2009.01.055.

[29] J. Prakash *et al.*, "Optical and surface enhanced Raman scattering properties of Au nanoparticles embedded in and located on a carbonaceous matrix," *Phys. Chem. Chem. Phys.*, vol. 18, no. 4, pp. 2468–2480, 2016, doi: 10.1039/C5CP06134B.

[30] "E.C. Le, Ru,E. Blackie, M. Meyer, P.G. Etchegoin J. Phys. Chem. C, 111 (2007), pp. 13794-13803".

[31] C. Li and M. Chen, "Active site-dominated electromagnetic enhancement of surface-enhanced Raman spectroscopy (SERS) on a Cu triangle plate," *RSC Adv.*, vol. 10, no. 69, pp. 42030–42037, 2020, doi: 10.1039/D0RA08477H.

[32] D. Zhang *et al.*, "The effect of solvent environment toward optimization of SERS sensors for pesticides detection from chemical enhancement aspects," *Sensors Actuators, B Chem.*, vol. 256, pp. 721–728, 2018, doi: 10.1016/j.snb.2017.09.209.